# Cross Correlating 21 cm Intensity Mapping fields with Kinematic Sunyaev-Zel'dovich Effect: Probing Missing Baryons at $z \sim 1-2$

Dongzi Li,[1,2] Ue-Li Pen,[3,4,5,1] Hong-Ming Zhu,[6,7] and Yu Yu[8]

[1]*Perimeter Institute for Theoretical Physics, 31 Caroline St. N., Waterloo, ON, N2L 2Y5, Canada*
[2]*University of Waterloo, 200 University Ave W, Waterloo, ON, N2L 3G1, Canada*
[3]*Canadian Institute for Theoretical Astrophysics, 60 St. George Street, Toronto, Ontario M5S 3H8, Canada*
[4]*Dunlap Institute for Astronomy and Astrophysics, 50 St. George Street, Toronto, Ontario M5S 3H4, Canada*
[5]*Canadian Institute for Advanced Research, CIFAR Program in Gravitation and Cosmology, Toronto, Ontario M5G 1Z8, Canada*
[6]*Key Laboratory for Computational Astrophysics, National Astronomical Observatories, Chinese Academy of Sciences, 20A Datun Road, Beijing 100012, China*
[7]*University of Chinese Academy of Sciences, Beijing 100049, China*
[8]*Key laboratory for research in galaxies and cosmology, Shanghai Astronomical Observatory, Chinese Academy of Sciences, 80 Nandan Road, Shanghai 200030, China*

(Dated: September 30, 2016)

The prominent defficiency of baryon contents in observations for $z \lesssim 2$ and its close correlation with baryon distributions, galaxy feedbacks and intergalactic medium conditions stand in the way of understanding structure evolution. To study the distribution of diffusive 'missing baryons', a large scale oriented probe, the kinematic Sunyaev-Zel'dovich (kSZ) effect on cosmic microwave background, was proposed. However, its faintness and lack of redshift require another signal to cross correlate with it. Previous proposals either require large sky galaxy spectroscopic surveys, or existing photemetric surveys combined with full ACTPol/CMB-S4 data to obtain persuasive results, which is hard to achieve in next five years. In this paper, a new possibility of cross correlating kSZ with HI density from 21cm Intensity Mapping surveys is discussed. The high effeciency and low facility requirements of the surveys make it possible for several ongoing experiments, eg. CHIME, to achieve large sky coverage and consistently measure $z \lesssim 2$ sky in next few years. Assuming realistic facility conditions and noise scales, we find that after retrieving noise smeared information on large scales with tidal coupling between scales, a minimum of $15$ S/N for both redshift 1 and 2 could be reached with CHIME + Planck. The fast construction of interferometers with longer baselines, eg. HIRAX, may foster the S/N to reach $50$ for redshift 2 with noise level of Planck.

PACS numbers:

## I. INTRODUCTION

For $z \lesssim 2$, large fractions of predicted baryon contents are missing in observations. The majority of them are believed to reside in warm-hot intergalactic mediums (WHIM) with typical temperature of $10^5$ K to $10^7$ K [1, 2]. High temperature and low density in the medium, as well as uncertainties in ionization states and metalicities, make it difficult to derive information from metal absroption lines. It is expected urgently for probes that not only trace the majority of the baryons, but also can be interpreted model-independently.

Among proposed probes, the kinematic Sunyaev-Zel'dovich (kSZ) effect [3–5] is a promising one. kSZ effect results from Compton scattering of cosmic microwave background (CMB) off free electrons. The radial velocity of electrons will give photon a Doppler shift and hence leads to a secondary anisotropy in CMB temperature. It is an ideal probe to tackle the problem: First, it contributes from all the free electrons, indicating the distribution of $90\%$ of the baryons in ionized states, leaving alone only less than $10\%$ of baryons that reside in stars, remnants, atomic and molecular gases [6]. Second, the signal is mainly influenced by electron density and radial velocity, regardless the temperature, pressure and metalicity, so no extra assumptions are needed to estimate baryon abundance. Third, the peculiar velocity is dominantly related to large scale structures, therefore the signal is less biased towards local mass contraction, and more indicative about diffusive distributions.

Attractive as it is, two drawbacks largely reduce the feasibility of harnessing kSZ signal. First, the signal is weak and hence suffers seriously from contaminations from primary CMB, facility noises, thermal SZ effect, CMB lensing, etc. Second, it is an integrated effect along line of sight, therefore, kSZ itself does not contain redshift information.

A straight-forward mitigation of the disadvantages is to cross correlate kSZ signal with another tracer, which has both large scale structure and redshift information. Previous work has proposed optical spectroscopic survey as an ideal tool [7–9]. However, first, it lacks detectable spectral lines in redshift $1.4-2.5$, therefore unable to consistently measure full $z < 2$ sky. Moreover, kSZ signal is more prominent in higher redshift, while it is extremely inefficient for spectroscopic surveys to cover large sky area for $z > 1$. Therefore this method is of no immediate access. Methods with lower facility requirements, such as cross correlating photo-z galaxies with kSZ [10, 11], depends on models of velocity fields, and demands next generation CMB facilities to achieve convincing S/N.

In this paper, a new possibility of cross correlating HI density field from 21 cm intensity mapping to kSZ signal is discussed. HI 21 cm spectra have accurate redshift information, and are fully accessible for $z \lesssim 2$. Intensity mapping survey, rather than distinguishing individual galaxies, integrates all weak signals in a pixel, which enables it to reach high S/N and scan large sky area in much shorter time. In the following few years, there will be several experiments producing data of large sky

area for redshift $\lesssim 2.5$ [12**?** , 13].

However, as feasibility is usually traded from data quality, there are three main challenges for the upcoming H I surveys in terms of cross correlation with kSZ. First, the integration of different signals will cause complicated foregrounds, which would smear the large scale structure in radial direction[14, 15]. Second, the angular resolution is also supressed by the integration, droping information of small scale structure in transverse plane. Third, till now, the proposed experiments all work on interferometers, which drain the largest scale structure on transverse plane due to the finite length of the shortest baseline.

On the other hand, the most prominate kSZ signals that could be distinguished from noises are mainly from $k_z \lesssim 0.1h/Mpc$ in radial direction with $l < 100$ and $l \sim 1000 - 2000$. These modes are partly damaged in intensity mapping due to the three challenges. In this paper, we evaluate the influence of the incompelete modes and partially recover the smeared large scale structures from their tidal influence on small scales[16, 17]. Final correlation is presented against different conditions.

The paper is organized as follows: In section II, we demonstrate given a density field, how to correlate it with kSZ signal in a holographic way similar to [8]. In section III, the weights of different Fourier modes on generating kSZ signals are discussed and used to evaluate existing modes in 21cm intensity mappings. In section IV, the method of 3D tidal reconstruction is introduced. Results of the reconstruction and cross correlation are presented in section V. And S/N is estimated via statistical error in section VI. Finally we conclude at section VII.

Notes: Throughout the paper, We use the $z = 1, 2$ output of six $N$-body simulations from the CUBEP$^3$M code [18], each evolving $1024^3$ particles in a $(1.2\mathrm{Gpc}/h)^3$ box. Simulation parameters are as follows: Hubble parameter $h = 0.678$, baryon density $\Omega_b = 0.049$, dark matter density $\Omega_c = 0.259$, amplitude of primordial curvature power spectrum $A_s = 2.139 \times 10^{-9}$ at $k_0 = 0.05\ \mathrm{Mpc}^{-1}$ and scalar spectral index $n_s = 0.968$.

## II. ALGORITHM: KSZ CROSS CORRELATION

In this section, we present a holographic method to cross correlate kSZ with a density field, following [8].

The CMB temperature fluctuations caused by kSZ effect is:

$$\Theta_{kSZ}(\hat{n}) \equiv \frac{\Delta T_{kSZ}}{T_{\mathrm{CMB}}} = -\frac{1}{c}\int d\eta g(\eta)\boldsymbol{p}_{\parallel}\ , \tag{1}$$

where $\eta(z)$ is the comoving distance at redshift z, $g(\eta) = e^{-\tau}d\tau/d\eta$ is the visibility function, $\tau$ is the optical depth to Thomson scattering, $\boldsymbol{p}_{\parallel} = (1+\delta)\boldsymbol{v}_{\parallel}$, with $\delta$ the electron overdensity, $\parallel$ indicates direction parallel to line of sight. We assume that $g(\eta)$ doesn't change significally in one redshift bin, and integrate $\boldsymbol{p}_{\parallel}$ along radial axis to get $\hat{\Theta}_{kSZ}$

Due to the cancellation of positive and negative velocity, direct cross correlation between kSZ signals and density contrast will vanish. However, taking advantage of the known redshift, we could at most maintain the one to one multiplication between velocity field and density contrast by linearly calculating the peculiar velocity and generating a mock kSZ signal. The basic procedure is as follows:

Assume we have a density contrast field $\delta = (\rho - \bar{\rho})/\bar{\rho}$, where $\bar{\rho}$ is the average density of a certain redshift slice.

(1) Estimate the velocity field:

In linear region, the continuity equation goes like: $\dot{\delta} + \nabla \cdot \boldsymbol{v} = 0$, where $\boldsymbol{v}$ is the peculiar velocity and $\delta$ is the matter overdensity. Therefore, linear velocity is estimated as:

$$\hat{v}_z(\boldsymbol{k}) = iaHf\delta(\boldsymbol{k})\frac{k_z}{k^2} \tag{2}$$

where $f = d\ln D/d\ln a$, $D(a)$ is the linear growth function, $a$ is the scale factor, $H$ is the Hubble parameter.

$v_z \propto k_z/k^2$, indicating the most prominent signal comes from small k mode, which corresponds to large scale structure.

(2) Filter the noise: The term $k_z/k^2$ in Eq.(2) will amplify noises in small k, which should be suppressed.

$$\hat{v}_z^c(\boldsymbol{k}) = \frac{\hat{v}_z(\boldsymbol{k})}{b(k_\perp, k_\parallel)}W(k_\perp, k_\parallel)\ , \tag{3}$$

Bias $b = P_{\hat{v}_z, v_z}/P_{v_z}$, Wiener filter $W = P_{v_z}/(P_{\hat{v}_z}/b^2)$.

(3) Calculate 2D kSZ map following Eq.(1).

(4) Calculate correlation coefficients:

Quantify tightness of correlation with:

$$r \equiv \frac{P_{recon,real}}{\sqrt{P_{recon}P_{real}}} \tag{4}$$

Where $\hat{\Theta}_{kSZ}$ is reconstructed signal and $\Theta_{kSZ}$ is original signal directly from simulations.

## III. CONDITION: KSZ + 21CM INTENSITY MAPPING

In this section, we discuss the origin of kSZ signal on different structure scales, compare it with scales resolvable in ongoing 21cm Intensity Mapping experiments, and give an intuitive picture of the possibility and difficulty of the cross correlation.

### A. kSZ properties

To understand what role each scale plays in generating kSZ signal, we write Eq.(1) in Fourier space.

The finite box size of 1200 Mpc only has notable influence on modes with $k \lesssim 0.005$. It is safe to assume minus infinity to plus infinity integration on $z$ direction for small scale modes.

Moreover, the term $a(z)H(z)f(z)$ in Eq.(2) does not vary much in one box, we assume it to be a constant for simplicity. Then the Fourier transformation is just the $k_z = 0$ mode of the momentum $p_\parallel(\boldsymbol{k})$ in Fourier space.

$$\begin{aligned}\Theta(\boldsymbol{\ell}) &\equiv \Theta(k_x\chi, k_y\chi, 0) \\ &\propto \int d^3k'\delta(\boldsymbol{\ell}/\chi - \boldsymbol{k}'_\perp, k'_\parallel)v_z(\boldsymbol{k'})\end{aligned} \tag{5}$$

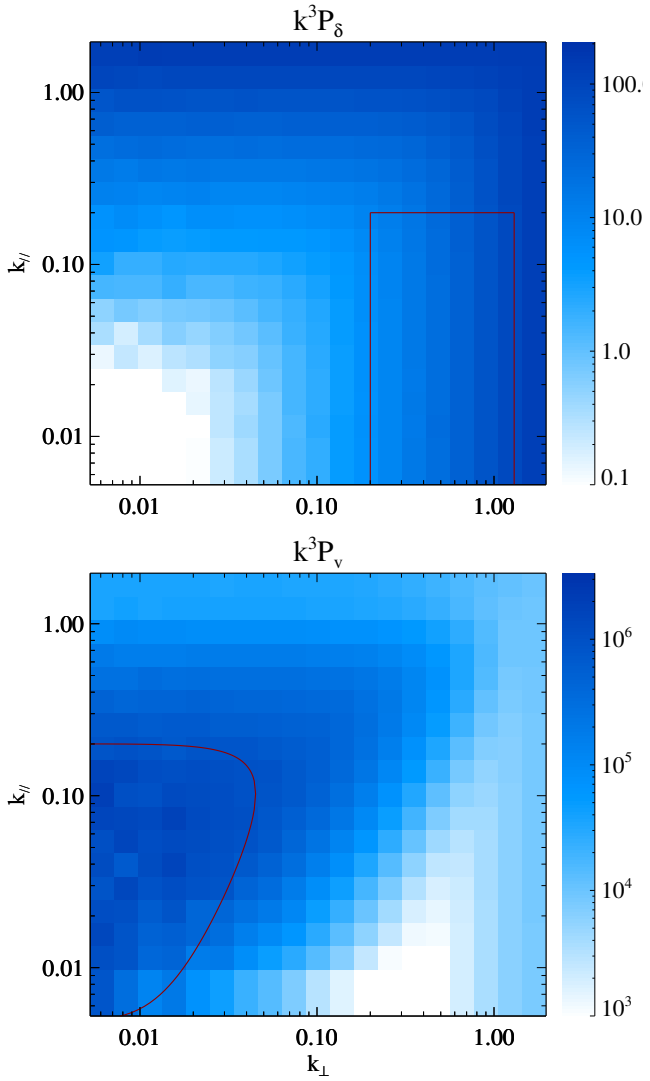


FIG. 1: Illustrating weights of different scales after integration. Demonstrated with data of redshift 1. (Top) The density variance $2\pi^2\Delta^2_\delta \equiv k^3 P_\delta$. (Bottom) The velocity variance $2\pi^2\Delta^2_{v_z} \equiv k^3 P_{v_z}$. (Red lines): Indicate most essential modes for generating kSZ signal in $\ell \sim 500 - 3000$.

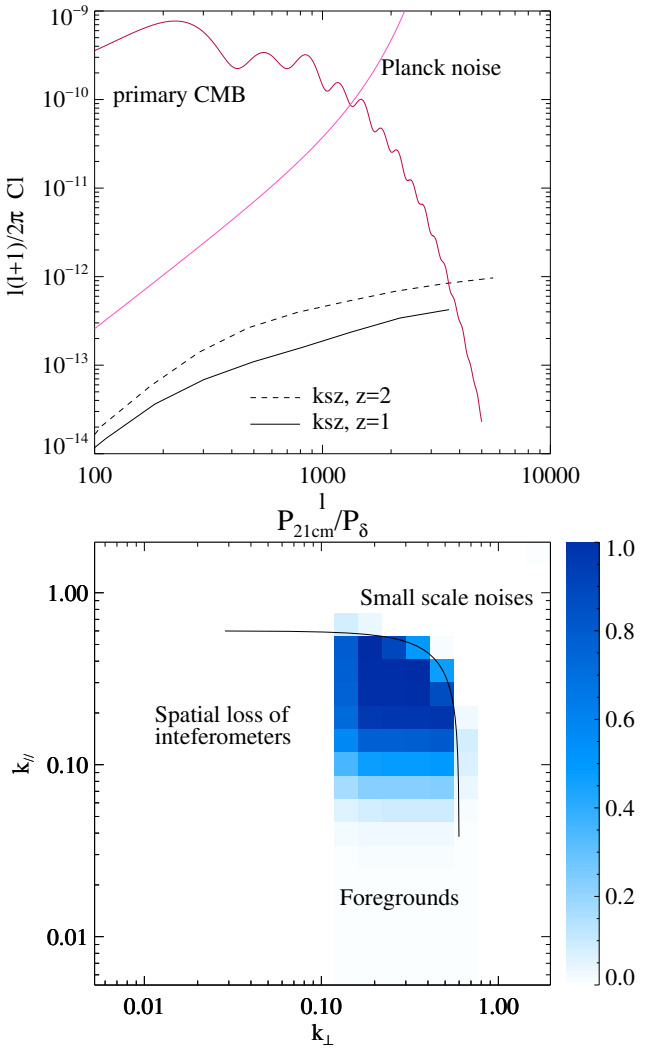


FIG. 2: (Top) Relative strength of angular powerspectrum between primary CMB, Planck noise in 217 GHz band, and kSZ effect in redshift 1 and 2. (Bottom) Available modes of density contrasts obtained in realistic 21cm Intensity Mapping experiments, with resolution of CHIME and high foregrounds ($R_\parallel = 15$ h/Mpc) in redshift 1. $P_{21cm}$ is the remaining density powerspectrum after noise substraction; $P_\delta$ indicates the powerspectrum of a intact density field.

An essential feature of Eq.(5) is that in transverse plane, density and velocity field of different scales are multiplied together, while in parallel direction, there is no coupling between different scales.

The relative strength of $|\delta(\boldsymbol{k})|$ and $|v_z(\boldsymbol{k})|$ in different scales are implied in Fig.1. and also implicit at Eq.(2), The velocity field contributes almost dominantly from large scale structures, leaving little contribution from $k_z > 0.2$ h/Mpc, $k_\perp > 0.02$ h/Mpc. This makes it roughly an ellipitical selection functions in the convolution — It selects $\delta$ with similar range of $k_z$ and $k_\perp \sim (\ell/\chi - 0.01)$ h/Mpc. Actually, the sharper $|v(\boldsymbol{k})|$ is, the more it ressembles a Delta Function peaked at $(k_\perp, k_\parallel) = (0.01, 0.1)$ h/Mpc. If we go into extreme:

$$\Theta(\boldsymbol{l}) \propto \int d^3k' \delta(\boldsymbol{\ell}/\chi - \boldsymbol{k}'_\perp, k'_\parallel)\delta^D(0.01, 0.1) \quad (6)$$

$$\sim \delta(\ell/\chi - 0.01, 0.1). \quad (7)$$

Therefore, when generating kSZ signals, it is crucial to have large scale modes for $v_z$. However, which scales matter most for $\delta(\boldsymbol{k})$ depends on the $\ell$ we look at.

To decide the targeted $\ell$ range, many factors needs to be taken into account: the strength of the primary CMB, facility limits, other fluctuations on CMB such as thermal SZ effect and CMB lensing. Consider using Planck [19] data in the 217 GHz band, where the tSZ signal vanishes, we demonstrate

the angular powerspectrum of primary CMB, facility noises (detailed calculations are shown in Section VI), and kSZ of redshift 1 and 2 in Fig.**??**. Only in the range of $\ell \sim 500-3000$, there is a chance for us to distinguish the kSZ signal.

In Fig.1, we roughly sketch the essential modes for $v_z(\boldsymbol{k})$ and $\delta(\boldsymbol{k})$ in red lines. In linear theory, velocity field of a certain scale only relates to identical scale of density field (see Eq.(2)). Therefore, an ideal density field should be intact in both regions.

Note: all the demonstration figures are towards redshift 1, however, there is only slight difference in redshift 2, which should not influence the qualitive analysis.

### B. 21 cm Intensity Mapping Properties

Main modes loss of ongoing 21cm intensity mapping experiments are demonstrated in this chapter with simple filters.

1. Small scale noises:

The finite spacial and velocity resolution of facilities import a cut off scale $k_{max}$ on both parallel and perpendicular directions, filtering out information of smaller scales. It is resembled with a Heaviside Function $H(k_{max}-k)$, dropping $k > k_{max}$.

2. Foreground noises:

Foregrounds from Galactic emissions, telescope noises, extragalactic radio sources and Radio recombination lines, could be three orders brighter than actual signals[14, 15]. The process of foreground removal, taking advantage of its low spectral degrees of freedom [20], will inevitably contaminates the smooth large scale structure in radial direction. To imitate the loss, a high pass filter $W_{fs}(k_\parallel) = 1 - e^{-k_\parallel^2 R_\parallel^2/2}$ is applied to density contraction.

3. Spatial loss of inteferometers:

Large scale structure in perpendicular plane, due to the smoothness, will appear sharp in the visibility function of interferometers after Fourier transformation. Unfortunately that sharp peak could not be resolved by interferometers due to the incomplete sampling caused by the finite length of the shortest baselines. Therefore, structures with angular sizes greater than a threshold $l_{min}$ will be lost.

In sum, the observed 21 cm density contrasts after all the loss will appear as

$$\delta_{nf}(\boldsymbol{k}) = \delta(\boldsymbol{k}) H(k_{max}-k) W_{fs}(k_\parallel) H(l-l_{min}), \quad (8)$$

The chosen parameters and reasons are presented in Table. I.

Demonstration of a filtered density field corresponding to $R_\parallel = 15$ Mpc/h, $k_{max} = 0.6$ h/Mpc in $z = 1$ is shown in Fig.**??**. Essential modes for density field are partly left, while the modes for velocity field are completely gone due to the spatial loss of inteferometers. Directly using the filtered density contrast to generate mock kSZ signal will yield $r < 0.2$ in Eq.(**??**)

Luckily, till now only linear theories are considered in reconstruction, while there are couplings between different scales in nonlinear theories. Identifying a single nonlinear effect will help us retrieve important modes for velocity reconstruction. Here, we present an algorithm to employ distortions from second order tidal coupling to solve for large scale structures [16, 17].

| | z=1 | | z=2 | |
|---|---|---|---|---|
| | high foreground | low foreground | high foreground | low foreground |
| [a] $R_\parallel$ Mpc/h | 15 | 60 | 10 | 40 |
| | CHIME | HIRAX | CHIME | HIRAX |
| [b] $k_{max}$ h/Mpc | 0.6 | 1.2 | 0.4 | 0.8 |
| [c] $\ell_{min}$ | 300 | | | |

[a]Foreground: smear $k_z \lesssim 0.08, 0.02, 0.12, 0.03$ h/Mpc respectively. Parameters based on [21–23]

[b]Small scale noises: based on CHIME[24] and HIRAX[13] with 100 m and 200 m longest baseline respectively.

[c]Spatial loss of inteferomenter: assuming shortest baseline of 20 m.

TABLE I: Parameter of different noise filtering.

## IV. ALGORITHM: COSMIC TIDAL RECONSTRUCTION

The evolution of small scale structure is modulated by large scale tidal force. We can select this effect and solve for the large scale potential.

Consider only the anisotropic influence from tidal force, the distortions on power spectrum can linearly be calculated as

$$\delta P(\boldsymbol{k},\tau)|_{t_{ij}} \;=\; \hat{k}^i \hat{k}^j t_{ij}^{(0)} P_{1s}(k,\tau) f(k,\tau) \quad (9)$$

where f is the linear coupling function; $P_{1s}(k,\tau)$ is the theoretical small scale linear powerspectrum; and $\delta P(\boldsymbol{k},\tau)$ is the real distortion from observations.

We can solve for the unknown quantity $t_{ij}$, which is the tidal force tensor defined as

$$t_{ij} = \Phi_{L,ij} - \nabla^2 \Phi_L \delta_{ij}^D/3 \quad (10)$$

$\Phi_{L,ij}$ is the second derivative of large scale potential, and i,j indicates $\hat{x}, \hat{y}, \hat{z}$ directions, $\delta^D$ is the Dirac function.

With $t_{ij}$, we calculate the variance of large scale potential $\Phi_L$ and get the large scale density contrast $\kappa_{3\mathrm{D}}$.

$$\kappa_{3\mathrm{D}} \sim \nabla^2 \Phi_L = \frac{3}{2} \nabla^{-2} \partial_i \partial_j t_{ij} \quad (11)$$

Since $f(k,\tau)$ increase with k in our interested scales, the distortions are more obvious in small scales. Therefore, the method mainly use the quadratic statistics on small scales to recover the large scale density field. It works best for close linear regions.

Programming steps:

(1) Gaussianize the field, taking $\delta_g = \ln(1+\delta)$. This is to allieviate the problem that filter $W_i$ in Eq.(14) heavily weights high density regions.

(2) Following gravitational lensing procedures, decompose the symmetric, traceless tidal force tensor into 5 components,

$$t_{ij} = \begin{pmatrix} \gamma_1 - \gamma_z & \gamma_\times & \gamma_2 \\ \gamma_\times & -\gamma_1 - \gamma_z & \gamma_y \\ \gamma_2 & \gamma_y & 2\gamma_z \end{pmatrix}. \quad (12)$$

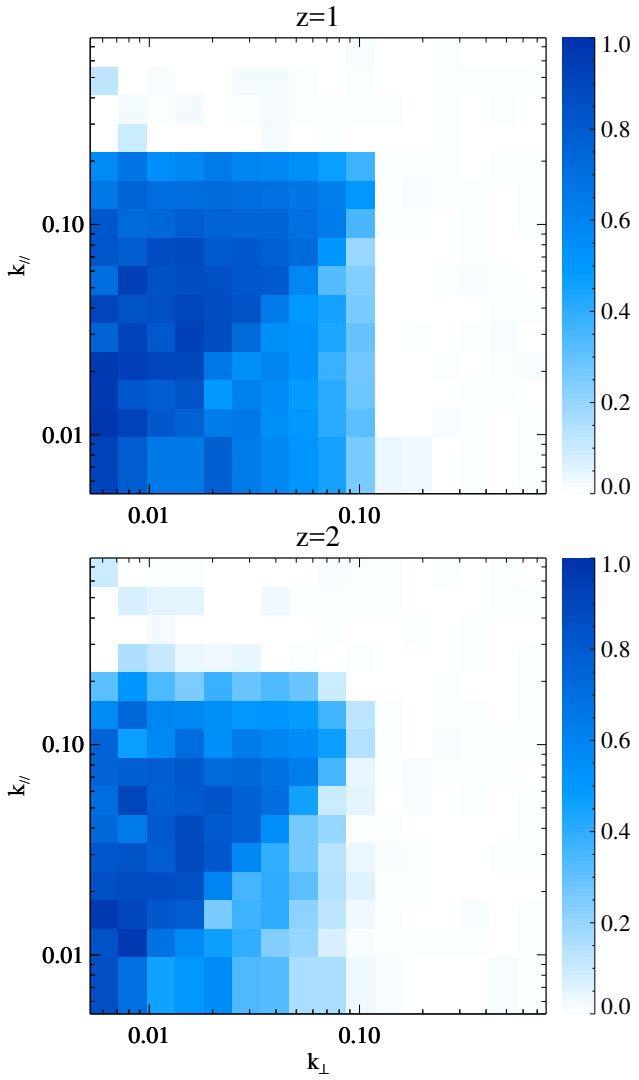


FIG. 3: Correlation coefficient r between reconstructed velocity field and real velocity field, assuming a baseline of 100m and serious foregrounds smearing $k_z$ below $0.08$ h/Mpc and $0.12$ h/Mpc of redshift 1 and 2 respectively.

(3) Select density distortions caused by tidal force, by convolving $\delta_g$ with a filter $W_i$ deduced from Eq.(9)

$$\delta_g^{w_i}(\boldsymbol{k}) = W_i(\boldsymbol{k})\delta_g(\boldsymbol{k}) \tag{13}$$

$$W_i(\boldsymbol{k}) = i\left[\frac{P(k)f(k)}{P_{tot}^2(k)}\right]^{\frac{1}{2}}\frac{k_i}{k} = S(k)\frac{k_i}{k}$$

$f(k) = 2\alpha(\tau) - \beta(\tau)d\ln P/d\ln k$ is again the coupling function, with $\alpha$ and $\beta$ related to linear growth funcion [17], and calculated to be (0.6, 1.3) for $z = 1$ and (0.4, 0.9) for $z = 2$. $P_{tot} = P + P_{noise}$ is the observed matter powerspectrum, and P is theoretical matter powerspectrum,

(4) Estimate the 5 tidal tensor components from quadratic statistics.

$$\begin{aligned}
\hat{\gamma}_1(\boldsymbol{x}) &= [\delta_g^{w_1}(\boldsymbol{x})\delta_g^{w_1}(\boldsymbol{x}) - \delta_g^{w_2}(\boldsymbol{x})\delta_g^{w_2}(\boldsymbol{x})],\\
\hat{\gamma}_2(\boldsymbol{x}) &= [2\delta_g^{w_1}(\boldsymbol{x})\delta_g^{w_2}(\boldsymbol{x})],\\
\hat{\gamma}_x(\boldsymbol{x}) &= [2\delta_g^{w_1}(\boldsymbol{x})\delta_g^{w_3}(\boldsymbol{x})],\\
\hat{\gamma}_y(\boldsymbol{x}) &= [2\delta_g^{w_2}(\boldsymbol{x})\delta_g^{w_3}(\boldsymbol{x})],\\
\hat{\gamma}_z(\boldsymbol{x}) &= \frac{1}{3}[(2\delta_g^{w_3}(\boldsymbol{x})\delta_g^{w_3}(\boldsymbol{x})\\
&\quad -\delta_g^{w_1}(\boldsymbol{x})\delta_g^{w_1}(\boldsymbol{x}) - \delta_g^{w_2}(\boldsymbol{x})\delta_g^{w_2}(\boldsymbol{x}))],
\end{aligned} \tag{14}$$

(5) Reconstruct large scale density contrast $\kappa_{3\mathrm{D}}$ from tidal tensor:

$$\begin{aligned}
\kappa_{3\mathrm{D}}(\boldsymbol{k}) = \frac{1}{k^2}\quad & [(k_1^2 - k_2^2)\gamma_1(\boldsymbol{k}) + 2k_1k_2\gamma_2(\boldsymbol{k})\\
& +2k_1k_3\gamma_x(\boldsymbol{k}) + 2k_2k_3\gamma_y(\boldsymbol{k})\\
& +(2k_3^2 - k_1^2 - k_1^2)\gamma_z(\boldsymbol{k})].
\end{aligned} \tag{15}$$

(6) Correct bias and suppress noise with a Wiener filter.

Due to the foregrounds, the noise in $z$ direction will be different from $x$,$y$ direction, therefore we apply an anisotropic Wiener filter.

$$\hat{\kappa}_c(\boldsymbol{k}) = \frac{\kappa_{3\mathrm{D}}(\boldsymbol{k})}{b(k_\perp, k_\parallel)}W(k_\perp, k_\parallel)\ , \tag{16}$$

Bias $b(k_\perp, k_\parallel) = P_{\mathrm{k3D},\delta}/P_\delta$ is the cross powerspectra between reconstructed field $\kappa$3D and original field $\delta$, Wiener filter $W(k_\perp, k_\parallel) = P_\delta/(P_{\mathrm{k3D}}/b^2)$.

Here $\hat{\kappa}_c$ is the output large scale density contrast we obtain from tidal reconstruction. We use it to calculate velocity $\hat{v}_z^{\mathrm{tide}}$.

## V. RESULTS

To avoid manipulating noises, we perform tidal reconstruction on most conservative estimates, i.e. $R_\parallel = 15$ Mpc/h, $k_{max} = 0.6$ h/Mpc, $\ell_{max} = 100$ for $z = 1$; and $R_\parallel = 10$ Mpc/h, $k_{max} = 0.4$ h/Mpc, $\ell_{max} = 100$ for $z = 2$.

The cross correlation between $\hat{v}_z^{tide}$ and $v_z$ are demonstrated in Fig.3. Important modes for velocity fields (within redline of Fig.1 lower label) are well extracted with correlations greater than 0.7. The reconstruction on $z = 2$ is slightly worse than $z = 1$ due to stronger foreground and lower resolution.

Combining reconstructed velocity field with density fields of different conditions, we get mock kSZ signals. Their correlation coefficients with exact kSZ are demonstrated in Fig.4. Even with identical tidal reconstructed velocity field, better foreground techneque can improve the correlation coefficient by 0.2. If the foreground is removed clean enough for more modes to be used in tidal reconstruction procedure, the improvement will be more notable. Resolution of facility will improve the reconstruction on higher $\ell$, consisting with previous analysis.

## VI. STATISTICAL ERROR AND S/N

Taking into account primary CMB and facility noises, the chance to seperate kSZ signal from statistical errors could be

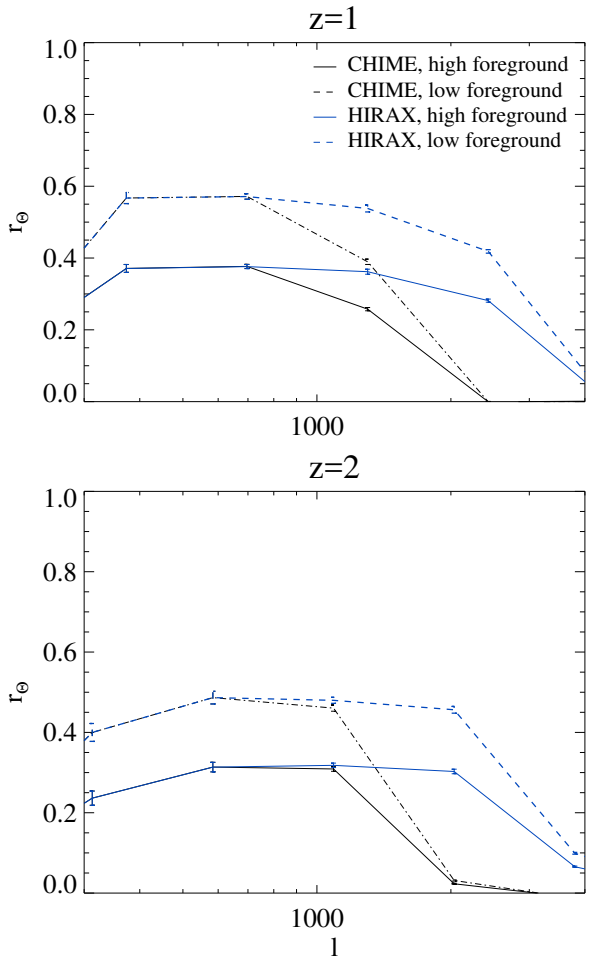


FIG. 4: The correlation coefficient r between real kSZ $P_{\Theta_{kSZ}}$ and reconstructed kSZ $P_{\hat{\Theta}_{kSZ}}$.

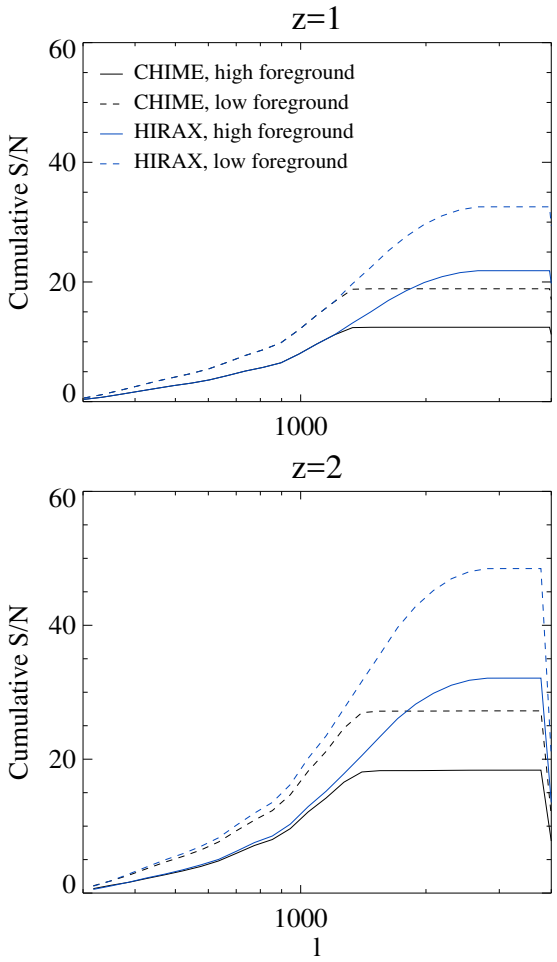


FIG. 5: Cumulative S/N, assuming Planck noise at 217 GHz, $f_{sky} = 0.8$.

estimated as:

$$\frac{S}{N} = \frac{C_l}{\Delta C_l} \simeq r\sqrt{(2\ell+1)\Delta l f_{\rm sky}}\sqrt{\frac{C_l^{\rm kSZ,\Delta z}}{C_l^{\rm CMB}+C_l^{\rm kSZ}+C_l^{\rm CMB,N}}} \quad (17)$$

Where $C_l^{\rm CMB}$ is the angular powerspectrum of primary CMB ; $C_l^{\rm CMB,N}$ indicates the facility noises; $C_l^{\rm kSZ,\Delta z}$ is the kSZ signal from a certain redshift bin; r is the correlation coefficients we get; $f_{\rm sky}$ is the percent of sky area covered by both surveys.

In our case, $C_l^{\rm CMB}$ is calculated from CAMB [25]. $C_l^{\rm CMB,N}$ is estimated with Planck results [19] at 217GHz. $C_l^{\rm CMB,N} = (\sigma_{p,T}\theta_{\rm FWHM})^2 W_l^{-2}$; where $\sigma_{p,T} = 8.7\mu K_{\rm CMB}$ is Sensitivity per beam solid angle, $\theta_{\rm FWHM} \sim 5'$ is the effective beam FWHM, $W_l = \exp[-\ell(\ell+1)/2\ell_{\rm beam}^2]$ is the smoothing window function, with $\ell_{\rm beam} = \sqrt{8\ln 2}/\theta_{\rm FWHM}$. We choose $f_{\rm sky} = 0.8$ according to claimed 21 cm intensity mapping survey area. $C_l^{\rm kSZ,\Delta z}$ is calculated within two bins of size 1200 Mpc/h, centered at redshift 1,2 respectively.

The cumulative S/N is demonstrated in Fig.5. The low correlation in $z = 2$ is compensated by the high electron density and the overall S/N could well reach 50 with HIRAX.

With noise level of Planck, the resolution of HIRAX already cover most important $\ell$s. However, with $4_{\rm th}$ generation facilities, more detectable modes will apprear in higher $\ell$s, and better S/N could be expected with longer baselines like SKA.

## VII. CONCLUSION

In this paper, we discuss the possibility of cross correlating kSZ signal with 21 cm intensity mapping to study baryon distributions. All the calculations are based on ongoing experiment condition and realistic noise scales. A holographic way of cross correlation is applied. Second order tidal coupling of different scales are employed to compensate for lost large scale modes. With existing Planck data, it is reasonable to expect at least 15 S/N with data from CHIME, and more optimistic estimates will yield 50 S/N for redshift 2 with HIRAX. The main obstacle for optimal correlation is lack of low $k_z$ high $k_\perp$ data due to foregrounds. This leads to information waste in the reconstructed velocity field. However, data from weak

lensing, photo-z galaxy surveys, which contains only large scale structure in z direction, may compensate for that.

This method is promising for its feasibility and model independence. CHIME already starts to collect data, and HIRAX is also in a close flight. It is reasonable to expect it to be tested within five years. Moreover, the method does not rely on assumptions about velocity fields or interstellar medium conditions. Less misunderstanding will appear while interpreting results. It is reasonable to expect it to be a new reliable attemp to study baryon distributions up to redshift 2 or higher. This will foster the understanding of baryonic feedbacks of galaxies, and the study intergalactic medium.

## VIII. ACKNOWLEDGE

We acknowledge discussions Wenkai Hu, Tianxiang Mao and Jiawei Shao. The simulations were performed on the BGQ supercomputer at the SciNet HPC Consortium. SciNet is funded by: the Canada Foundation for Innovation under the auspices of Compute Canada; the Government of Ontario; the Ontario Research Fund – Research Excellence; and the University of Toronto. Research at the Perimeter Institute is supported by the Government of Canada through Industry Canada and by the Province of Ontario through the Ministry of Research & Innovation. The Dunlap Institute is funded through an endowment established by the David Dunlap family and the University of Toronto.

[1] U.-L. Pen, ApJ **510**, L1 (1999), astro-ph/9811045.
[2] A. M. Sołtan, A&A **460**, 59 (2006), astro-ph/0604465.
[3] R. A. Sunyaev and Y. B. Zeldovich, Comments on Astrophysics and Space Physics **4**, 173 (1972).
[4] R. A. Sunyaev and I. B. Zeldovich, MNRAS **190**, 413 (1980).
[5] E. T. Vishniac, ApJ **322**, 597 (1987).
[6] M. Fukugita and P. J. E. Peebles, ApJ **616**, 643 (2004), astro-ph/0406095.
[7] N. Hand, G. E. Addison, E. Aubourg, N. Battaglia, E. S. Battistelli, D. Bizyaev, J. R. Bond, H. Brewington, J. Brinkmann, B. R. Brown, et al., Physical Review Letters **109**, 041101 (2012), 1203.4219.
[8] J. Shao, P. Zhang, W. Lin, Y. Jing, and J. Pan, MNRAS **413**, 628 (2011), 1004.1301.
[9] M. Li, R. E. Angulo, S. D. M. White, and J. Jasche, MNRAS **443**, 2311 (2014), 1404.0007.
[10] J. C. Hill, S. Ferraro, N. Battaglia, J. Liu, and D. N. Spergel, ArXiv e-prints (2016), 1603.01608.
[11] S. Ferraro, J. C. Hill, N. Battaglia, J. Liu, and D. N. Spergel, ArXiv e-prints (2016), 1605.02722.
[12] Y. Xu, X. Wang, and X. Chen, ApJ **798**, 40 (2015), 1410.7794.
[13] http://www.acru.ukzn.ac.za/ hirax/.
[14] T. Di Matteo, B. Ciardi, and F. Miniati, MNRAS **355**, 1053 (2004), astro-ph/0402322.
[15] K. W. Masui, E. R. Switzer, N. Banavar, K. Bandura, C. Blake, L.-M. Calin, T.-C. Chang, X. Chen, Y.-C. Li, Y.-W. Liao, et al., ApJ **763**, L20 (2013), 1208.0331.
[16] U.-L. Pen, R. Sheth, J. Harnois-Deraps, X. Chen, and Z. Li, ArXiv e-prints (2012), 1202.5804.
[17] H.-M. Zhu, U.-L. Pen, Y. Yu, X. Er, and X. Chen, ArXiv e-prints (2015), 1511.04680.
[18] J. Harnois-Déraps, U.-L. Pen, I. T. Iliev, H. Merz, J. D. Emberson, and V. Desjacques, MNRAS **436**, 540 (2013), 1208.5098.
[19] Planck Collaboration, R. Adam, P. A. R. Ade, N. Aghanim, M. Arnaud, M. Ashdown, J. Aumont, C. Baccigalupi, A. J. Banday, R. B. Barreiro, et al., ArXiv e-prints (2015), 1502.01587.
[20] E. R. Switzer, T.-C. Chang, K. W. Masui, U.-L. Pen, and T. C. Voytek, ApJ **815**, 51 (2015), 1504.07527.
[21] K. W. Masui, E. R. Switzer, N. Banavar, K. Bandura, C. Blake, L.-M. Calin, T.-C. Chang, X. Chen, Y.-C. Li, Y.-W. Liao, et al., ApJ **763**, L20 (2013), 1208.0331.
[22] E. R. Switzer, K. W. Masui, K. Bandura, L.-M. Calin, T.-C. Chang, X.-L. Chen, Y.-C. Li, Y.-W. Liao, A. Natarajan, U.-L. Pen, et al., MNRAS **434**, L46 (2013), 1304.3712.
[23] J. R. Shaw, K. Sigurdson, M. Sitwell, A. Stebbins, and U.-L. Pen, Phys. Rev. D **91**, 083514 (2015), 1401.2095.
[24] K. Bandura, G. E. Addison, M. Amiri, J. R. Bond, D. Campbell-Wilson, L. Connor, J.-F. Cliche, G. Davis, M. Deng, N. Denman, et al., in *Society of Photo-Optical Instrumentation Engineers (SPIE) Conference Series* (2014), vol. 9145 of *Society of Photo-Optical Instrumentation Engineers (SPIE) Conference Series*, p. 22, 1406.2288.
[25] A. Lewis, A. Challinor, and A. Lasenby, Astrophys. J. **538**, 473 (2000), astro-ph/9911177.